T-cell Receptor Therapy Targeting Mutant Capicua Transcriptional Repressor in Experimental Gliomas

Michael Kilian[1,2,3], Mirco Friedrich[1,2], Khwab Sanghvi[1,2,3], Edward Green[1], Stefan Pusch[4,5], Daisuke Kawauchi[6,7], Martin Löwer[8], Jana K. Sonner[1], Christopher Krämer[1], Julia Zaman[3,4], Stefanie Jung[1], Michael O. Breckwoldt[1,9], Gerald Willimksy[10,11,12], Stefan B. Eichmüller[13], Andreas von Deimling[4,5], Wolfgang Wick[14,15], Felix Sahm[4,5], Michael Platten[1,2,16], and Lukas Bunse[1,2]

ABSTRACT

Purpose: Gliomas are intrinsic brain tumors with a high degree of constitutive and acquired resistance to standard therapeutic modalities such as radiotherapy and alkylating chemotherapy. Glioma subtypes are recognized by characteristic mutations. Some of these characteristic mutations have shown to generate immunogenic neoepitopes suitable for targeted immunotherapy.

Experimental Design: Using peptide-based ELISpot assays, we screened for potential recurrent glioma neoepitopes in MHC-humanized mice. Following vaccination, droplet-based single-cell T-cell receptor (TCR) sequencing from established T-cell lines was applied for neoepitope-specific TCR discovery. Efficacy of intraventricular TCR-transgenic T-cell therapy was assessed in a newly developed glioma model in MHC-humanized mice induced by CRISPR-based delivery of tumor suppressor–targeting guide RNAs.

Results: We identify recurrent capicua transcriptional repressor (CIC) inactivating hotspot mutations at position 215 CICR215W/Q as immunogenic MHC class II (MHCII)-restricted neoepitopes. Vaccination of MHC-humanized mice resulted in the generation of robust MHCII-restricted mutation-specific T-cell responses against CICR215W/Q. Adoptive intraventricular transfer of CICR215W-specific TCR-transgenic T cells exert antitumor responses against CICR215W-expressing syngeneic gliomas.

Conclusions: The integration of immunocompetent MHC-humanized orthotopic glioma models in the discovery of shared immunogenic glioma neoepitopes facilitates the identification and preclinical testing of human leukocyte antigen (HLA)-restricted neoepitope-specific TCRs for locoregional TCR-transgenic T-cell adoptive therapy.

Introduction

Cellular therapies are a rapidly developing field in cancer immunotherapy (1). For the development of chimeric antigen receptor (CAR)-expressing T and natural killer (NK) cells, bispecific T-cell engagers (BiTes), and T-cell receptor (TCR)-transgenic T cells, the identification of tumor-specific targets is crucial. In immune-privileged primary brain tumors such as gliomas, identification of suitable targets, however, remains a major challenge due to a paucity of tumor-specific neoepitopes and a lymphodepleted tumor microenvironment (2–4). Hence, there is a need to carefully assess the therapeutic potential of neoepitopic shared driver mutations in gliomas. Glioma subtypes are molecularly defined by characteristic driver mutations, such as mutations in isocitrate dehydrogenase (IDH) and Histone H3 (5). In a hypothesis-driven approach, oncogenic mutated proteins such as IDH1R132H and H3.3K27M have been shown to harbor immunogenic neoepitopes that can be targeted by therapeutic vaccines in preclinical models and phase I clinical trials (6–11). In principle, immunogenic shared driver mutations may not only be utilized for targeted off-the-shelf immunotherapies but also serve as a role model to establish preclinical workflows for adoptive therapy using neoepitope-specific TCR-transgenic T cells, which also

[1]DKTK Clinical Cooperation Unit Neuroimmunology and Brain Tumor Immunology, German Cancer Research Center (DKFZ), Heidelberg, Germany. [2]Department of Neurology, Mannheim Center for Translational Neuroscience (MCTN), Medical Faculty Mannheim, University of Heidelberg, Mannheim, Germany. [3]Faculty of Biosciences, Heidelberg University, Heidelberg, Germany. [4]DKTK Clinical Cooperation Unit Neuropathology, German Cancer Research Center (DKFZ), Heidelberg, Germany. [5]Department of Neuropathology, Heidelberg University Hospital, University of Heidelberg, Heidelberg, Germany. [6]Division of Pediatric Neurooncology, German Cancer Research Center (DKFZ), Heidelberg, Germany. [7]Hopp Children's Cancer Center Heidelberg (KiTZ), Heidelberg, Germany. [8]TRON - Translational Oncology at the University Medical Center of Johannes Gutenberg University, Mainz, Germany. [9]Department of Neuroradiology at the Neurology Center, Heidelberg University Hospital, Heidelberg, Germany. [10]Institute of Medical Immunology, Charité-Universitätsmedizin Berlin, corporate member of Freie Universität Berlin and Humboldt-Universität zu Berlin, Berlin, Germany. [11]German Cancer Research Center (DKFZ), Heidelberg, Germany. [12]German Cancer Consortium (DKTK), Partner Site Berlin, Berlin, Germany. [13]Research Group GMP & T Cell Therapy, German Cancer Research Center (DKFZ), Heidelberg, Germany. [14]Department of Neuro-oncology and National Center for Tumor Diseases, Heidelberg University Hospital, University of Heidelberg, Heidelberg, Germany. [15]DKTK Clinical Cooperation Unit Neurooncology, German Cancer Research Center (DKFZ), Heidelberg, Germany. [16]Helmholtz Institute for Translational Oncology (HI-TRON) Mainz, Mainz, Germany.

Note: Supplementary data for this article are available at Clinical Cancer Research Online (http://clincancerres.aacrjournals.org/).

Corresponding Author: Lukas Bunse, DKTK Clinical Cooperation Unit Neuroimmunology and Brain Tumor Immunology, German Cancer Research Center (DKFZ), Im Neuenheimer Feld 280, 69120 Heidelberg, Germany. E-mail: l.bunse@dkfz.de

Clin Cancer Res 2022;28:378–89

doi: 10.1158/1078-0432.CCR-21-1881

Translational Relevance

Oligodendrogliomas are intrinsic brain tumors that are incurable. In a screen for potential immunogenic glioma neoepitopes we identify recurrent capicua transcriptional repressor (CIC) inactivating hotspot mutations at position 215 CICR215W/Q expressed in a subset of oligodendrogliomas as an immunogenic MHC class II (MHCII)-restricted neoepitope. Using a newly developed glioma model in MHC-humanized mice induced by CRISPR-based delivery of tumor suppressor–targeting guide RNAs, we show that adoptive intraventricular transfer of CICR215W-specific T-cell receptor (TCR)–transgenic T cells exerts antitumor responses against CICR215W-expressing syngeneic gliomas. In combinatorial immunotherapeutic regimes including immune checkpoint inhibition and irradiation, an increased rate of long-term surviving mice was observed, providing new evidence that MHCII-restricted TCR-transgenic locoregional T-cell therapy shows preclinical therapeutic efficacy in difficult-to-treat primary central nervous system (CNS) tumors.

incorporate private neoepitopes representing the majority of neoepitopes in gliomas (12, 13).

Seventy percent of 1p19q-codeleted oligodendrogliomas, tumors with low mutation burden, carry capicua transcriptional repressor (CIC)-inactivating mutations (14–16). Importantly, 5% to 10% of these oligodendrogliomas harbor a recurrent monomorphic CIC hotspot mutation at position 215 where arginine (R) is substituted to tyrosine (W) or glutamine (Q). It is thought that CIC acts as tumor suppressor in gliomas in which decreased CIC expression levels are correlated with poor outcome. In 1p19q-codeleted oligodendrogliomas, missense, in-frame deletions, nonsense, and frame-shift mutations cooccur to LOH of chromosomes 1p and 19q (17, 18). Conversely, in glioblastomas, continuous proteasome-mediated degradation by the E3 ligase PJA1 results in negligible levels of the tumor suppressor CIC (17). In this study we set out to develop a workflow for the detection of potential novel shared neoantigens and neoepitope-specific TCRs for adoptive therapy of TCR-transgenic T cells in astrocytomas and oligodendrogliomas.

Materials and Methods

Mice and cell lines

HLA-A*0201 HLA-DRA*0101 HLA-DRB1*0101 transgenic mice devoid of mouse MHC [A2.DR1 mice, B6-Tg(HLA-DRA*0101,HLA-DRB1*0101)^{1Dmz} Tg(HLA-A/H2-D/B2M)^{1Bpe} H2-Ab^{tm1Doi} B2m^{tm1Unc} and B6-Tg(HLA-DRA*0101, HLA-DRB1*0101)^{1Dmz} Tg(HLA-A/H2-D/B2M)^{1Bpe} H2-Ab1^{tm1Doi} B2m^{tm1Unc} H2-D1^{tm1Bpe}] were provided by M. Berard (Institute Pasteur; ref. 19) and bred at the DKFZ animal facility. NOD.Cg-*Prkdc*^{scid} *Il2rg*^{tm1Wjl}/SzJ (NSG; ref. 20) mice came from the Jackson Laboratory and were bred at the DKFZ animal facility. Eight- to 16-week-old mice were assigned to age-matched and sex-matched experimental groups. C57BL/6-Tg(HLA-IEd alpha/HLA-DRB1*0401-I-Ed beta) were obtained from Taconic. Mice were housed under Specific and Opportunistic Pathogen Free (SOPF) conditions and 12-hour day/night cycle.

Hek Phoenix Eco cells were cultured in DMEM supplemented with 10% FBS, 100 U/mL penicillin, and 100 μg/mL streptomycin (P/S, Sigma-Aldrich) and selected for transgene expression with hygromycin (Sigma-Aldrich). A2.DR1 glioma cell lines were generated as described below and cultured in DMEM supplemented with 10% FBS, P/S. Transfected cell lines were selected with 9 μg/mL blasticidine (Gibco; see below). Cells were tested for *Mycoplasma* contamination before inoculation.

MHC binding prediction

MHC binding prediction was performed using NetMHC 4.0 (21, 22) and NetMHCIIpan 4.0 (23). Input files were 27-mers listed in Supplementary Table S1. For NetMHC 4.0 we screened for 8- to 12-mers. For NetMHCIIpan 4.0 we screened for 15-mers (Supplementary Table S1).

Peptides

P53, CICR215Q, and CICR215W 27-mers were synthesized in house. CICR215W 15-mer peptides and mouse myelin oligodendrocyte glycoprotein (MOG) were synthesized by Genscript. All peptides are listed in Supplementary Table S1. Lyophilized peptides were reconstituted in DMSO (10%), subsequently diluted with PBS, and stored at −80°C.

Vaccination of mice

A2.DR1 or C57B/6J mice were vaccinated with 100 μg respective peptide emulsified in 100 μL 1:1 PBS:Montanide-ISA51 (Seppic). Mice received 50 μL each in the lateral pectoral regions. Three hundred nanograms rmGM-CSF (Immunotools) in PBS was subcutaneously injected between injection sites, and Aldara cream containing 5% imiquimod (Meda Pharma) was applied at shaved injection site. Mice were boosted at day 10 with peptide and Aldara cream. Mice were terminated at day 21.

Generation of A2.DR1 gliomas

A2.DR1 gliomas were generated using the CRISPR-Cas9–based triple gene knockout approach described previously (24). Briefly, A2.DR1 P0 pups were electroporated with *p53, NF1*, and *Pten* guide RNAs cloned into pX330 plasmids (Addgene). To control for successful electroporation the plasmid pT2K IRES-luciferase was coelectroporated. P0 A2.DR1 mice were anesthetized with 2% isoflurane and medially injected at lambda: −3.6 and dorsal/ventral (D/V): −0.7 with 1 μg DNA in 1 μL. After injection, electric square pulses were delivered laterally using forceps-like electrodes [35 mV (VZ), 50 ms-on, 950 ms-off, 5 pulses]. Mice were subjected to bioluminescence imaging of luciferase activity (IVIS, Perkin Elmer) 7 days after electroporation to ensure delivery of the constructs. Mice were imaged by magnetic resonance (MR) two times (6 weeks and 12) after electroporation. Tumors were excised when mice showed signs of neurologic deficit (between 90 and 120 days). Tumors were mashed through a 100-μm cell strainer and reinjected subcutaneously into the flank of NSG mice. When tumors reached 1 cm in diameter, tumors were excised, and a single-cell suspension was obtained as described above. Cells were cultured in DMEM supplemented with 10% FBS and P/S for at least three passages to ensure removal of contaminating stromal cells. Gioma cell line M7 was selected for further experiments due to growth characteristics.

Intracranial tumor cell inoculation

A total of 2×10^4 A2.DR1 glioma cells were diluted in 2 μL sterile PBS (Sigma-Aldrich) and stereotactically implanted into the right hemisphere of 7- to 14-week-old male A2.DR1 mice (coordinates: 2 mm right lateral of the bregma and 1 mm anterior to the coronal

suture with an injection depth of 3 mm below the dural surface), using a 10-μL Hamilton microsyringe driven by a fine step stereotactic device (Stoelting). Tumor cell inoculation was performed under anesthesia and mice received analgesics for 2 days after operation. Mice were checked daily for tumor-related symptoms and sacrificed when tumor burden and stop criteria were met or mice showed signs of neurologic deficit.

MRI

MRI was carried out by the small animal imaging core facility at DKFZ using a Bruker BioSpec 3 Tesla (Ettlingen, Germany) with ParaVision software 360 V1.1 or at the department of neuroradiology, University Hospital Heidelberg (9.4 T Bruker Biospec 9/20).

For imaging, mice were anesthetized with 3.5% sevoflurane or 1% to 2% isoflurane in air. For lesion detection T2-weighted imaging was performed using a T2-TurboRARE sequence: TE = 48 ms, TR = 3,350 ms, FOV 20 × 20 mm, slice thickness 1.0 mm, averages = 3, Scan Time 3 minutes 21 seconds, echo spacing 12 ms, rare factor 8, slices 20, image size 192 × 192. Tumor volume was determined by manual segmentation using Bruker ParaVision software 6.0.1 or OsiriX.

Irradiation

The head of tumor-bearing mice was irradiated under fully antagonizable anesthesia using a MultiRad225 (Precision X-Ray). Mice were irradiated with 4 Gy at day 11, 12, and 13 after tumor inoculation (total dose 12 Gy).

Therapeutic adoptive T-cell transfer

T cells were transduced with the CIC clonotype 2 (CT2) TCR or Flu control TCR as described below. After 40 hours, T cells were stained and sorted for $CD3^+$, GFP^+ T cells using a FACSAriaII cell sorter (BD Biosciences). Sorted T cells were expanded for 3 days using CD3/CD28 antibodies as described below and 20 U hIL2. Directly before injection, T cells were mixed with 20 μg/mL of PD-1 and CTLA-4 blocking antibodies each (PD-1: clone RMP1–14, CTLA-4: clone 9D9, both BioXCell). A total of 4×10^5 T cells were stereotactically injected in 4 μL PBS into the left ventricle of A2.DR1 glioma-bearing mice at a speed of 1 μL per second (coordinates: 0.5 mm left lateral of the bregma with an injection depth of 1.8 mm below the dural surface). The syringe was kept in the injection side for 3 minutes. T-cell inoculation was performed under anesthesia and mice received analgesics for 3 days after operation. Mice were randomized according to tumor size at first MRI. Experimentators were blinded to treatment allocation. Sample size was calculated with the help of a biostatistician using R version 3.4.0. Assumptions for power analysis were as follows: alpha error: 5%; beta error: 20%. Values for SD and differences between experimental groups were based on previous experiments.

Where applicable, mice were treated with 250 μg αPD-1 and 100 μg αCTLA-4 or isotype controls (all BioXCell) 12, 15, 19, and 22 days after tumor inoculation.

In vivo proliferation assay

Transduced A2.DR1 T cells were expanded as above for 5 days and labeled with 1 μmol/L Cell Trace Far Red (Thermo Fisher Scientific) and intravenously injected into A2.DR1 mice. Twenty-four hours after transfer, mice were injected with 50 μg αCD40 antibody (clone: FGK4.5, BioXCell) and 50 μg CICR215W or MOG peptide. Four days after T-cell transfer, spleens were extracted and analyzed by flow cytometry.

Isolation of immune cells from spleen, lymph nodes, and tumor

Tumor-free mice were sacrificed by cervical dislocation and spleen and lymph nodes were extracted and mashed through a 70-μm strainer. Contaminating erythrocytes were lysed using ACK lysis buffer (Gibco).

For tumor-infiltrating lymphocytes (TIL) from brain tumors, mice were anesthetized and perfused with 20 mL PBS. The right hemisphere was extracted and digested with 50 μg/mL Liberase (Sigma) for 30 minutes and subsequently mashed through 100-μm and 70-μm cell strainers to obtain a single-cell suspension. Myelin was removed using a 30% continuous percoll gradient.

ELISpot was performed as previously described (6). Briefly, wetted ELISpot plates (MAIPSWU10, Millipore) were incubated with 100 μL 15 μg/mL IFNγ coating antibody (AN-18, Mabtech) and incubated overnight at 4°C. Cells from spleen and lymph nodes from vaccinated mice were extracted at day 21 after vaccination and resuspended in RPMI-1640 supplemented with 10% FBS, P/S as above, 50 μmol/L beta-mercaptoethanol (Sigma), 2 mmol/L L-glutamine, 25 mmol/L Hepes, 1 mmol/L sodium pyruvate (all Invitrogen), and 0.1 mmol/L nonessential amino acids (NEAA, Lonza; called T-cell medium, TCM). IFNγ coating antibody was removed and ELISpot plates were blocked with TCM. Three hundred thousand to 600,000 cells were plated, and peptides were added at 10 μg/mL. For positive control, 20 ng/mL phorbol 12-myristate 13-acetate (PMA) and 1 μg/mL ionomycin were used. Plates were incubated for 40 hours. Cells were removed and the plate was incubated with 1 μg/mL biotinylated IFNγ detection antibody (R4–6A2, Mabtech) in PBS with 0.5% FBS for 2 hours at room temperature. The detection antibody was removed and wells were incubated with 1 μg/mL streptavadin–alkaline phosphatase (ALP; Mabtech) in PBS with 0.5% FBS for 1 hour. Streptavidin-ALP was removed and plate was incubated with ALP development buffer (Bio-Rad) until distinct spots emerged. Spots were quantified with an ImmunoSpot Analyzer (Cellular Technology Ltd).

Generation of CicR215W-expressing cell lines

cDNA of murine Cic was provided by S. Pusch. The R215W mutation was introduced using the Q5 Site-Directed Mutagenesis Kit (New England Biolabs) by changing the codon 215 from nucleotide sequence CGG to TGG. The mutated gene was introduced into a modified pMXs-IRES-BsdR [Cell Biolabs, Inc.; Gateway Cassette was introduced in multiple cloning site (MCS) prior to Gateway cloning] using the Gateway cloning system (Thermo Fisher Scientific). A2.DR1 glioma cells were transfected using FuGene HD transfection reagent (Promega) according to manufacturer's protocol. Cells were selected with 9 μg/mL blasticidin (Sigma-Aldrich) 72 hours after transfection.

Generation of T-cell lines and TCR sequencing

CICR215W reactive T-cell lines were obtained as described previously (6). Briefly, splenocytes from A2.DR1 vaccinated mice were isolated and cultured for 7 days in TCM containing 10 μg/mL CICR215W peptide. Medium was exchanged weekly after 7 days and supplemented with 3% ConA supplement (kindly provided by W. Osen) and 15 mmol/L α-methylmonnopyranoside (α-MM, Sigma-Aldrich). T cells were restimulated with irradiated (30 Gy) autologous splenocytes from naïve A2.DR1 mice loaded with 2 μg/mL peptide every 4 weeks.

For deep TCR sequencing, T-cell lines after the second restimulation were used. DNA was isolated (QIAmp DNA Mini Kit, Qiagen) and submitted for murine ImmunoSEQ (Adaptive). For single-cell

VDJ sequencing, T-cell lines were pooled after the second restimulation and subjected to an IFNγ secretion assay (Miltenyi) according to manufacturers' protocol and sorted for IFNγ$^+$ CD4$^+$ T cells (for staining, see below) on a FACSAriaII cell sorter (BD Biosciences). Single-cell VDJ analysis was performed using the 10x technology and customized primers (Supplementary Table S3). The generated library was sequenced on a NextSeq 550 system and subsequently analyzed through the cell ranger pipeline 1.1 (10x Genomics). One thousand, six hundred and seventy cells with productive V-J spanning pair were retrieved.

Transduction of murine T cells

A retroviral construct was used for TCR transduction of primary murine T cells. First, the variable chain of respective TCRs was synthesized by Eurofins and subsequently cloned into a vector containing the murine constant alpha and beta chains. Subsequently, the full-length TCR was cloned into pMXS-TCR-IRES-GFP using the Gateway cloning system (Thermo Fisher Scientific).

Plates for T-cell activation were coated with 8 μg/mL anti-hamster IgG for 3 hours at 37°C and subsequently incubated with 0.1 μg/mL αCD3e (clone 145–2C11, eBioscience) at 4°C for 45 minutes. A2.DR1 splenocytes were harvested as described above. T cells were isolated using MagniSort Mouse T cell Enrichment Kit according to manufacturer's protocol and incubated in TCM with 1×10^5 IU/mL IL2 and 1 μg/mL αCD28 (clone 37.51, BioLegend) on αCD3e-coated cell culture plates overnight. HEK Phoenix Eco cells were seeded at a density of 3.5×10^5 cells/mL and transfected the next day with 12 μg DNA per 10 mL using FuGene (Promega) at a ratio of 1:4 DNA:Fugene according to manufacturer's protocol. Medium was changed after 24 hours and virus was harvested after 48 hours. The supernatant containing the virus was filtered through a 0.45 μm strainer and added to Retronectin (Takara)-coated cell culture plates (16 μg/mL Retronectin in PBS, 2 hours, 37°C). The virus was centrifuged at 4,000 rpm for 1 hour at room temperature. A total of 6×10^6/mL T cells were added to fresh virus and centrifuged at 2,300 rpm for 1 hour at room temperature. T cells were incubated for 5 hours at 37°C and resuspended in TCM supplemented with 20 IU/mL IL2. T cells were used for subsequent assays after 36 to 40 hours.

Coculture assays

T cells were transduced as described above. Splenocytes from A2.DR1 mice were isolated, irradiated (30 Gy), and loaded with 10 μg/mL peptide. Transduced T cells were added in a 1:1 ratio, incubated overnight, and subsequently stained for IFNγ expression. Tumor lysate was generated by three repeated thaw/freeze cycles. Bone marrow–derived dendritic cells (DC) were generated by extracting fresh bone marrow cells from hip and femur of A2.DR1 mice. Cells were incubated for 7 days with 20 ng/mL GM-CSF and 20 ng/mL IL4. DCs were loaded for 16 hours with tumor lysate from equal amounts of A2.DR1 CICR215W or wild-type (WT) cells and subsequently cocultured with transduced T cells at a 1:1 ratio.

NFAT activation assay

TCR-transgenic T cells were obtained as described above and cotransduced with an nuclear factor of activated T-cells (NFAT) reporter cloned into GatewayTM donor vector pDONR, seeded as described above with irradiated splenocytes and incubated for 8 hours. Nano-Glo (Promega) reagents were used according to manufacturer's instructions. Luciferase activity was measured using a Pherastar plate reader (BMG Labtech).

Flow cytometry

Murine cells were blocked with rat anti-mouse CD16/32 (0.5 μg per well, eBioscience) and stained with respective antibodies at diluations according to manufacturers' protocols: CD45-BV510 (30-F11, BioLegend), CD4–antigen-presenting cell (APC), CD4-BV510 (both RM4–5, BioLegend), CD8-Percp-Cy5.5 (53–7.7, eBioscience), CD3-FITC, CD3-BV421 (both 17A2, BioLegend), IFNγ-PE, IFNγ-APC (XMG1.2, BioLegend), HLA-A2-APC (BB7.2, BioLegend), HLA-DR-Percp eFl710 (L243, BioLegend), Ly6C-APC (KK1.4, BioLegend), CD11B-PE-Dazzle 594 (M1/70, BioLegend), Cxcl9-PE (MIG-2F5.5, BioLegend), I-A/I-E-AF700 (M5/114.15.2, BioLegend), CD11C-BV785 (N418, BioLegend). eFluor 780 fixable viability dye (eBioscience) was used according to manufacturer's protocol to exclude dead cells. For intracellular staining, cells were incubated at 37°C with 5 μg/mL Brefeldin A (Sigma) and respective stimulus (10 μg/mL for peptides, see also Elispot section) for 4 to 6 hours. Intracellular staining was performed using eBioscience Intracellular Fixation & Permeabilization Buffer Set for cytokines according to manufacturer's protocol. Nonfixed samples were acquired immediately, and fixed samples were acquired within 48 hours on a FACS Canto II (BD Biosciences) or a BD AriaII.

Histology

Brains from perfused A2.DR1 glioma-bearing mice were stored in Tissue-Tek OCT compound (Sakura) at −80 °C and cut into 6- to 8-μm slices using a cryotome (Leika). For immunofluorescence staining, slides were air dried, fixed with ice-cold methanol, and blocked for 2 hours with normal goat serum (Sigma). Slides were incubated overnight with the respective primary antibody (polyclonal Cic AB, 1:1000, Abcam; DRB1.01, L243, BioLegend) in blocking buffer. The slides were then incubated with the respective primary or secondary antibody for 1 hour (F4/80-APC, BM8, BioLegend, 1:200; goat-anti-rabbit, 1:300, AF488, Thermo Fisher Scientific; goat-anti-mouse AF488, 1:300, Thermo Fisher Scientific) and mounted using DAPI-containing mounting medium (Invitrogen). Images were acquired within 6 hours on a Cellobserver (Zeiss) or LSM700 confocal microscope (Zeiss).

Hematoxylin and eosin (H&E) staining was performed as previously described (6). Briefly, 8-μm slides were fixed with Roti-Histofix 4.5%. H&E staining was performed using hematoxylin and bluing reagent for 4 minutes.

Western blot

Protein was isolated by cell lysis using RIPA buffer (Thermo Fisher Scientific) for 20 minutes and centrifugation to remove debris. Protein concentration was determined via bicinchoninic acid (BCA) assay (Thermo Fisher Scientific). Fifteen micrograms whole protein were diluted in Laemmli sample buffer containing 2-mercaptoethanol, denatured for 5 minutes at 95°C, and electrophoretically separated on acrylamide-polyacrylamide SDS-containing gels. Proteins were blotted onto nitrocellulose by Western blot analysis at 1.5 mA cm^{-2} for 1 hour. After blocking with 5% milk powder in 0.5 M TBS, pH 7.4, 1.5 M NaCl, 0.05% Tween 20 (TBS-T), membranes were incubated with the primary antibody (polyclonal Cic AB, 1:1000, Abcam) in TBS-T with 5% milk powder overnight. As loading control, goat αGAPDH (1:5,000, Linaris) was used. Secondary horseradish peroxidase–conjugated antibodies were anti-rabbit (1:2,000, GE Healthcare) and anti-goat (1:2,000, Santa Cruz Biotechnology). Chemiluminescent development was done using enhanced chemiluminescence (ECL) or ECL prime (both Amersham).

qRT-PCR

Primers used for qRT-PCR are shown in Supplementary Table S2. RNA from cells or tissue was extracted using RNeasy Mini kit (Qiagen) and cDNA was obtained from 1 μg RNA using the High-Capacity cDNA Reverse Transcription Kit (Applied Biosystems). qRT-PCR was performed using primaQuant qPCR CYBR-Green-Master Mix with ROX (Steinbrenner) and samples were run on a QuantStudio 3 Real-Time PCR System (Applied Biosystems via Thermo Fisher Scientific). All samples were analyzed in quadruplicates and melting curves were considered to evaluate PCR reactions. C_t values were normalized to *GAPDH*.

Mutation detection and copy-number alteration

RNA or DNA was isolated from freshly isolated tumors from *in vivo* passage or from cells grown as monolayer using the RNeasy Mini Kit or DNeasy Blood & Tissue Kit (Qiagen), respectively, according to manufacturers' instructions. As germline control, DNA extracted from spleen of healthy mice was used. Libraries were sequenced on an Illumina NovaSeq (2 × 50 nt). DNA- and RNA-derived sequence reads were aligned to the mm9 genome as described previously (25).

Detection of mutations and copy-number calling was performed as described previously (25). Genes exhibiting copy-number alterations were annotated with their respective chromosomal location and transcript length by accessing the Biomart database in R (www.biomart.org) and using the Ensembl mouse genome (GRCm38.p6) as reference. The corresponding circos plot was plotted using the circlize package in R (26).

Statistics

Data are represented as individual values or as mean ± SEM. Group sizes (*n*) and applied statistical tests are indicated in each figure legend. Significance was assessed by either unpaired *t* test analysis or one-way ANOVA with Tukey test for multiple comparison indicated in figure legends. Log-rank Mantel–Cox test was used to examine survival differences. Statistics were calculated using GraphPad Prism 9.0.

Study approval

All animal procedures followed the institutional laboratory animal research guidelines and were approved by the governmental authorities (Regional Administrative Authority Karlsruhe, Germany).

Data availability

RNA sequencing (RNA-seq) and exome sequencing (ExomeSeq) data that support the findings of this study are deposited here: https://www.ncbi.nlm.nih.gov/sra/PRJNA773808. Cell lines will be provided by the corresponding author upon reasonable request. All additional datasets generated or analyzed during this study are included in this published article (and its Supplementary Data files).

Results

We screened potential immunogenic targets frequently mutated in oligodendrogliomas and astrocytomas [World Health Organization (WHO) grade 2–4; refs. 27, 28] by predicting HLA-A2– and HLA-DR1–binding affinities (NetMHC4.0 and NetMHCIIpan4.0). We identified five neoantigens predicted to strongly bind HLA-A2, including two point mutations in CIC and three in tumor protein 53 (TP53); all with considerable binding affinity difference compared with their wildtype counterparts (Supplementary Fig. S1A; Supplementary Table S1). To cover all potential epitopes, we vaccinated MHC-humanized transgenic A2.DR1 (HLA-A*0201/DRB1*0101) mice with the mutated 27-mer peptide of each potential target (**Fig. 1A**). While the peptides encompassing TP53 point mutations did not elicit a mutation-specific IFNγ response, peptides carrying the amino-acid exchange R to W or Q at position 215 in the CIC 27-mer peptide (CIC215W/Q) induced a mutation-specific IFNγ response (**Fig. 1B** and **C**; Supplementary Fig. S1B and S1C). Remarkably, restimulation of splenocytes with the complete 15-mer CICR215W peptide library did not result in IFNγ release, indicating a long MHC class II (MHCII)-restricted minimal epitope rather than a short MHC class I (MHCI)-restricted neoepitope (Supplementary Fig. S1D). Accordingly, IFNγ production in T cells from vaccinated A2.DR1 mice was limited to $CD4^+$ T cells after restimulation with CICR215W peptide (**Fig. 1D** and **E**). Of note, we did not observe IFNγ-positive cells in HLA-DR4 transgenic mice (Supplementary Fig. S1E). In two independent oligodendroglioma cohorts, position 215 was found to be a mutational hotspot in the *CIC* gene resulting either in CICR215W or CICR215Q, with approximately 2% of all WHO grade 2 gliomas carrying this mutation with an enrichment (3.5%–6.0%) in oligodendrogliomas (**Fig. 1F** and **G**). Since the CICR215W peptide led to significantly stronger immune responses than the CICR215Q mutation in A2.DR1 mice, we further focused on this target for subsequent experiments.

Preclinical assessment of brain tumor–specific immunotherapies in A2.DR1 mice has been hampered by the lack of appropriate tumor models. We thus generated experimental gliomas in A2.DR1 mice by applying a previously described CRISPR-Cas9–based genetic approach enabling somatic deletion of tumor suppressors *Neurofibromin 1* (*Nf1*), *Phosphatase and tensin homolog* (*Pten*), and *Trp53* (24) to newborn pups. This triple-knockout in the forebrain caused the formation of brain tumors after 3 months and lethal tumor growth after 4 to 5 months. After passaging the tumor cells in NSG mice and *in vitro*, generated tumors maintained their histologic integrity (**Fig. 2A**). The histopathologic morphology resembled an oligosarcoma phenotype. Mutational profiling of the cell line and the secondary tumors grown in NSG mice revealed a low mutational load with 37 mutations of which only seven were acquired during six *in vitro* passages (**Fig. 2B**). Of note, from an immunologic perspective, the mutational load was similar to human oligodendrogliomas, albeit usage of different oncogenic driver mutations (29). ExomeSeq of the cell line verified the CRISPR-Cas9–mediated knockout of all three genes (**Fig. 2C**; Supplementary Fig. S2A). About 10% of the total genes showed copy-number alterations (Supplementary Fig. S2B and S2C).

We next assessed the spontaneous immune cell infiltration of orthotopically injected experimental A2.DR1 gliomas in an untreated state. High T-cell infiltration of $CD8^+$ as well as $CD4^+$ T cells was observed, making this model suitable for targeted immunotherapeutic interventions (**Fig. 2D**). Of note, flow cytometric analysis and IHC staining revealed that the tumor cell line was negative for MHCII expression (**Fig. 2E**; Supplementary Fig. S2D). For *in vivo* targeting, we stably overexpressed CicR215W in the A2.DR1 glioma cell line (**Fig. 2F**; Supplementary Fig. S2E and S2F). Of note, the human and murine CIC proteins are highly conserved around position 215, with an identical peptide sequence of the selected CicR215W/CICR215W 27-mer peptide. Therefore, we overexpressed murine point–mutated *Cic* in the A2.DR1 glioma cell line.

Therapeutic peptide vaccinations in brain tumors rely on the induction of a meaningful peripheral T-cell response and sufficient T-cell trafficking into the immune-privileged CNS. In contrast, locoregional delivery of CAR-transgenic T cells has demonstrated strong preclinical efficacy in human brain tumor patient-derived

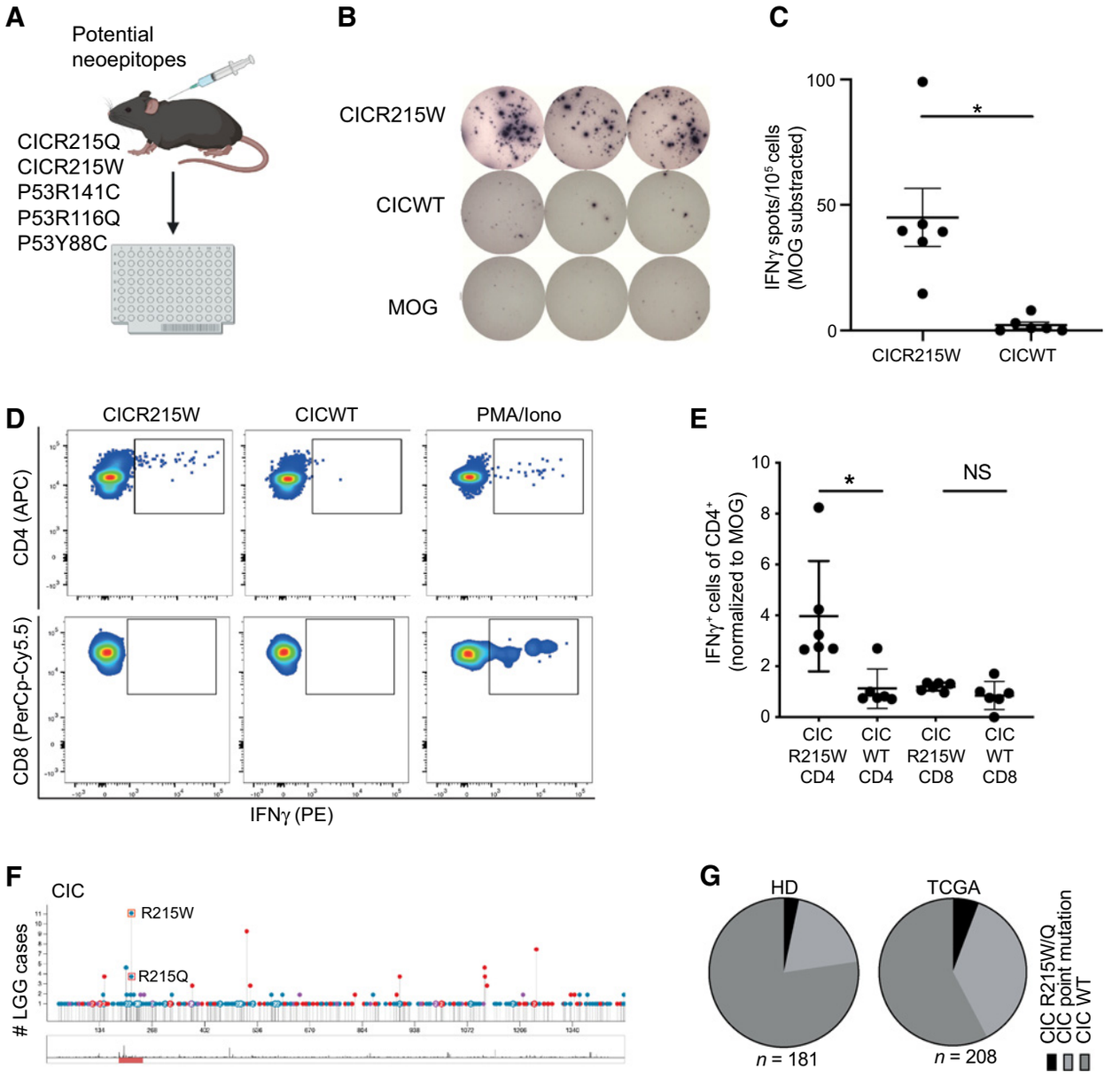

Figure 1.

Identification of CICR215W/Q point mutations as potential target for targeted immunotherapy. **A,** Experimental overview. Peptides harboring potential glioma-related neoepitopes were used for vaccination of A2.DR1 MHC-transgenic mice. **B,** Representative ELISpot assay of splenocytes isolated from CICR215W vaccinated mice restimulated for 48 hours with the indicated peptide. **C,** Quantification of data shown in **B**, $n = 6$ mice. **D,** Representative flow cytometric analysis of splenocytes from CICR215W vaccinated mice restimulated for 24 hours with the indicated 27-mer peptide and intracellularly stained for IFNγ production. **E,** Quantification of data shown in **D**, $n = 6$ mice. NS, not significant. **F,** The Cancer Genome Atlas (TCGA) analysis of the LGG dataset ($n = 516$); frequent mutations in the peptide position 215 are shown. **G,** Proportion of patients with CIC215-mutated tumors in the TCGA oligodendroglioma ($n = 208$) and Heidelberg oligodendroglioma ($n = 181$) cohorts. **C** and **E,** Data are represented as individual values and mean ± SEM. Statistical significance was determined by paired two-tailed Student *t* test.

xenografts (PDX; refs. 30–32). To translate this concept to MHCII-restricted TCRs, we generated CICR215W-reactive T-cell lines from splenocytes of vaccinated A2.DR1 mice via peptide-specific clonal expansion. T-cell lines from 5 mice were subjected to an IFNγ capture assay and cytokine-producing T cells were sorted and used for droplet-based single-cell TCR sequencing (scTCR-seq; **Fig. 3A**). ScTCR-seq showed an oligoclonal TCR repertoire in the T-cell pool (**Fig. 3B**). TCRβ sequencing of individual mice revealed high heterogeneity between different mice with one to two clones being highly prevalent (13%–78%) in each mouse (**Fig. 3B**). Strikingly, the TCR sequence of CT2 was shared between 4 out of 5 mice (with a frequency of 0.002% to 48.781%; Supplementary Fig. S3A). To assess if CT2 is CICR215W-

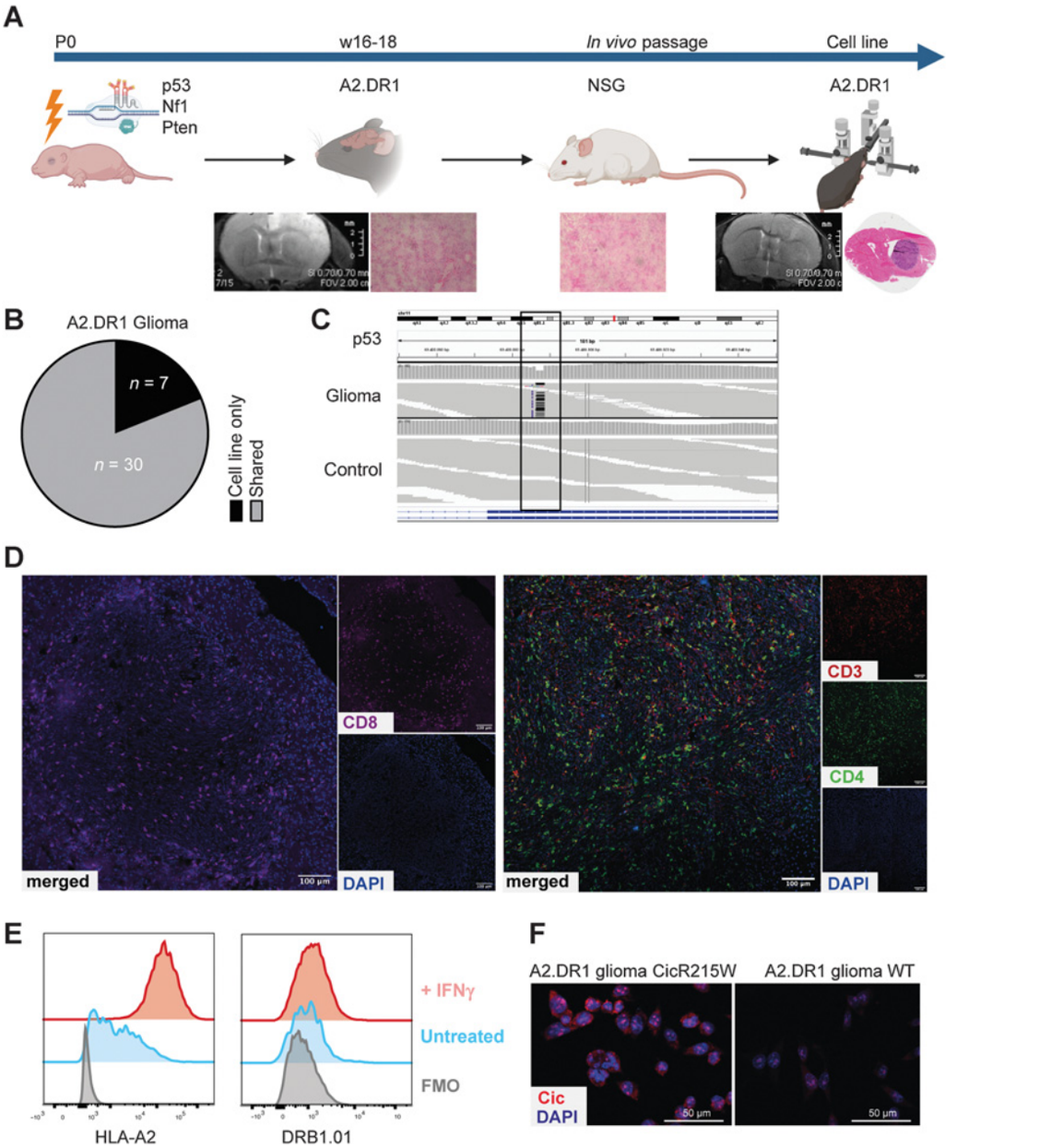

Figure 2.

Establishment of an A2.DR1 MHC-humanized glioma model. **A,** Experimental overview. P0 A2.DR1 pups were electroporated with plasmids encoding for CRISPR-Cas9 and 3 guide RNAs (gRNA) targeting p53, Nf1, and Pten. Growing tumors were excised, passaged in NSG mice, and used to generate a cell line that was reimplanted into adult A2.DR1 mice. MRI and H&E histology are shown for respective tumor stages. **B,** Pie chart depicting the proportions of mutations that are shared by the parental tumor and *ex vivo* passaged cell line or that are newly acquired after *in vitro* passage. **C,** Verification of the CRISPR-mediated functional knockout of p53 in the A2.DR1 glioma cell line. **D,** Representative immunofluorescence images of A2.DR1 glioma orthotopically injected into the brain of adult A2.DR1 mice, 20 days after injection. **E,** MHC expression of the A2.DR1 glioma cell line, incubated for 24 hours with recombinant murine IFNγ. FMO, fluorescence minus one control. **F,** Immunofluorescence image of CicR215W overexpressing A2.DR1 glioma cells.

reactive, we retrovirally transduced primary murine A2.DR1 T cells. Coexpression of GFP via an internal ribosomal entry site (IRES) allowed for the detection of transduced T cells (**Fig. 3C**). In fact, all top 3 TCR clones (CT1–3) identified by scTCR-seq showed stable IFNγ release upon restimulation with the mutated peptide in $CD4^+$ T cells that was comparable with an influenza virus (Flu)-specific TCR used as positive control (**Fig. 3D**; Supplementary Fig. S3B). Interestingly, T cells modified to express the shared TCR CT2 showed the most potent IFNγ response as well as NFAT activation in an NFAT-reporter assay (**Fig. 3D** and **E**; Supplementary Fig. S3B). Stimulation of CT2-transduced T cells with DCs loaded with CICR215W A2.DR1 glioma lysate lead to a mutation-specific IFNγ response (**Fig. 3F**), indicating

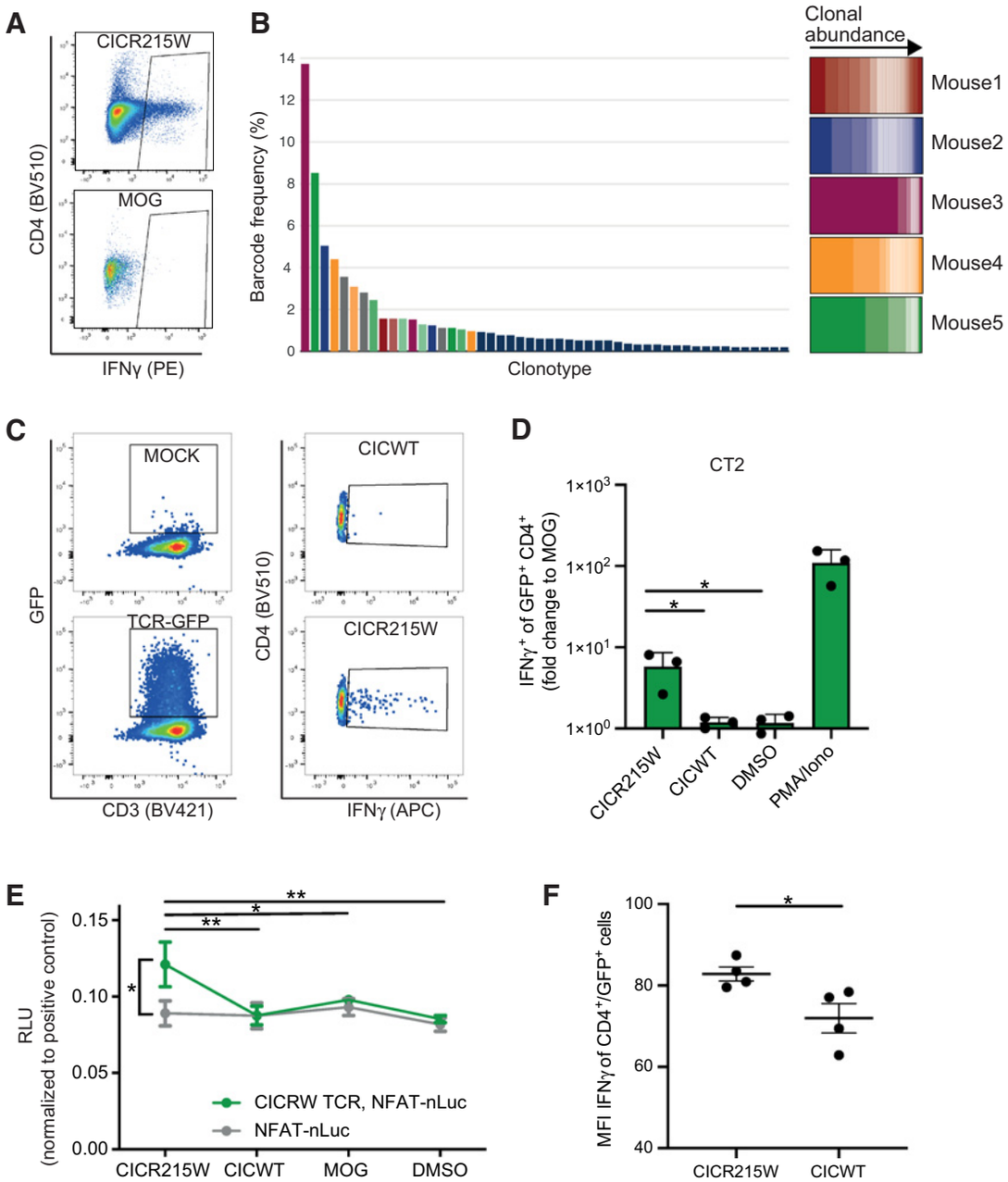

Figure 3.

Discovery and validation of CICR215W-reactive TCRs. **A,** T cells pooled from 5 individual T-cell lines generated from CICR215W vaccinated mice were subjected to an IFNγ-secretion assay, sorted for IFNγ-producing $CD4^+$ T cells and subsequently used for single-cell VDJ sequencing using the 10x Genomics platform. IFNγ staining by flow cytometry is shown. **B,** Left, clonotype distribution of **A**; right, color-coded abundance of clones in individual mice determined by TCRβ deep sequencing. **C,** Validation of α-CICR215W-TCR-transduced (CT2) $CD4^+$ T cells. Left, coexpression of GFP as reporter for TCR expression in α-CICR215W-TCR-transduced T cells as determined by flow cytometry. Mock, transduction control. Right, IFNγ production of GFP^+ α-CICR215W-TCR-transduced T cells after restimulation with irradiated splenocytes pulsed with the indicated peptides. **D,** IFNγ production of TCR-transduced T cells restimulated with irradiated splenocytes pulsed with the indicated peptide. $n = 3$ biological replicates. **E,** NFAT-reporter assay of CT-2 TCR- and NFAT-reporter transduced T cells, restimulated for 4 hours with irradiated splenocytes pulsed with the respective peptide, measured by luciferase signal. $n = 3$ technical replicates. **F,** IFNγ secretion of CT2 transduced T cells cocultured with DCs loaded with lysate from CicR215W or CicWT A2.DR1 glioma cells. $n = 4$ biological replicates. MFI, mean fluorescence intensity. **D–F,** Data are represented as individual values (**D**, **F**) and mean ± SEM. Statistical significance was determined by one-way ANOVA with Tukey test. RLU, relative light unit.

an endogenous processing of the neoepitope by professional APCs in an MHCII-dependent manner.

Common efficacy readouts for MHCI-restricted TCR-transgenic T cells are *in vitro* killing assays using MHCI-proficient target-expressing tumor cell lines. Even though some tumor cells do express MHCII themselves, thus far, it remains elusive if Th cells are able to directly recognize tumor cells and exert effector functions that are measurable *in vitro* (33). Moreover, evidence of *de novo* MHCI-restricted T-cell responses upon MHCII-restricted peptide vaccination exist, (34), suggesting stromal MHCII expression as prerequisite for MHCII-restricted T-cell therapy to be effective. Therefore, we aimed to assess the CICR215W-specific reactivity of TCR-transgenic T cells in experimental A2.DR1 glioma *in vivo*. CT2 as the most reactive clone was chosen for subsequent experiments. Strong IL2-dependent activation and expansion of T cells is a prerequisite for retroviral TCR transduction of murine T cells but at the same time drives PD-1 and CTLA-4 upregulation. To attenuate intratumoral exhaustion, immune checkpoint blocking (ICB) antibodies α-mPD-1, α-mCTLA-4 were applied (**Fig. 4A**). Pretreatment of T cells with ICB resulted in increased *in vitro* IFNγ response to the mutated peptide even after 5 days of expansion whereas untreated T cells were not able to induce an antigen-specific IFNγ response anymore (Supplementary Fig. S3C). Intravenously injected T cells expressing CT2 demonstrated prolonged *in vivo* proliferation in response to the peptide, insuring stable functionality of the TCR-transduced T cells (**Fig. 4B**; Supplementary Fig. S3B and S3D). As intraventricular injection of tumor-reactive transgenic T cells has been shown to be superior to systemic injection (31, 32, 35), we used stereotactic injection of TCR-transduced and ICB pretreated T cells into the contralateral ventricle of CicR215W^{+} A2.DR1 glioma-bearing mice. Two subsequent injections of CT2-TCR-transgenic T cells led to an increased median survival of 33 days compared with 29 days in the control group with no neurologic symptoms observed (**Fig. 4C**). Endpoint flow cytometric analysis revealed the prevalence of CICR215W-reactive transgenic T cells 15 days after the last injection in the tumor and control hemisphere. Only negligible numbers of transferred T cells could be detected in the cervical and deep cervical lymph nodes, leading to the assumption that the adoptively transferred CT2-TCR-transgenic T cells predominantly remain restricted to the CNS (Supplementary Fig. S3E). The adoptive transfer of CICR215W-reactive T cells led to an overall increase of T-cell infiltration into the tumor (**Fig. 4D**) and an increase of the Ly6C^{high} monocyte-derived myeloid cells expressing the T cell attracting chemokine CXC-ligand 9 (Cxcl9) and MHCII (**Fig. 4E** and **F**). In order to improve efficacy, we combined the adoptive transfer of CICR215W-reactive T cells with additional immunotherapeutic interventions. ICB has previously been shown to lead to durable antitumor responses in experimental glioma models (36, 37). However, in the here applied genetically driven A2.DR1 glioma model, the combination of αPD-1/αCTLA-4 with an adoptive transfer of TCR-transgenic T cells with irrelevant specificity did not improve survival of glioma-bearing mice (Supplementary Fig. S3F). The combination of ICB with CICR215W-reactive T cells led to 12.5% (1/8) long-term survivors (Supplementary Fig. S3F). Irradiation therapy is part of the standard-of-care treatment and frequently applied in treatment of recurrent gliomas. Synergisms with immunotherapeutic interventions and the respective underlying mechanisms have been extensively studied (38). Applying a fractionated irradiation with up to 12 Gy moderately prolonged survival in our humanized glioma model (4 to 5 days). Additive adoptive transfer of CICR215W-reactive transgenic T cells led to prolonged survival compared with noninjected or control-TCR injected mice with 16.7% long-term survivors (**Fig. 4G**).

Discussion

Immunotherapeutic interventions have now been established in many cancer entities with an emerging and promising focus on genetically manipulated cellular therapies (1, 39). Preclinical and casuistic clinical studies using CAR T cells showed efficacy in murine and human brain tumors, respectively (31, 32, 40). However, as CAR T-cell therapy is limited to surface antigens, epitopes are often tumor-associated but not -specific. When targeting tumor-associated antigens that are not exclusive to the tumor, on-target adverse events such as neurotoxicity have been reported (41, 42). Conversely, TCR-transgenic T-cell therapy allows for targeting intracellular, tumor exclusive neoepitopes (43, 44). First trials with TCR-engineered T cells targeting cancer-testis antigens have shown clinical responses against solid tumors like melanoma (45, 46). Nonetheless, identification of suitable targets remains challenging, specifically for tumors with low mutational burden. Two recent studies demonstrated the successful induction of T-cell responses by personalized peptide vaccines against MHCII-restricted neoantigens (12, 13). In these trials, neoepitopes were exclusively private. Therefore, transgenic-TCR therapy targeting neoepitopic shared driver mutations presented on common human leukocyte antigens, harbors the potential of potent off-the-shelf cellular immunotherapy.

Using an MHC-humanized mouse model, we demonstrated immunogenicity of the common amino acid exchange CICR215W/Q in the CIC protein, identifying it as a targetable neoantigen in oligodendrogliomas. Whereas previous reports targeting shared glioma antigens have made use of neoantigen-specific vaccination (6, 7, 9, 47), we further exploited an MHC-humanized mouse model for next-generation retrieval and preclinical assessment of brain-tumor–reactive TCRs, easily transferable into clinical application for TCRs specifically binding HLA-A2– and HLA-DR1–restricted tumor antigens. Using droplet-based scTCR-seq, we were able to retrieve functional TCRs from independent mice specifically reactive against the mutated peptide. Our novel glioma model resembles the low mutational load and aggressive growth of human gliomas in an MHC-humanized, but fully immunocompetent background, making it advantageous to chemically-induced hypermutated syngeneic mouse models (36, 37) or PDX-derived cell lines in immunodeficient mice (48).

CD4^{+} T-cell–restricted immune responses have already been shown to lead to durable tumor regression in preclinical models (6, 34); however, durable clinical efficacy in brain tumors still needs to be proven. Here we show that locoregional delivery of preactivated neoepitope-specific CD4^{+} T cells alone leads to prolonged survival in an orthotopic brain tumor model. As previously reported, MHCII expression on the tumor cell surface was dispensable for eliciting a CD4^{+} T cell–specific antitumor response (6, 49–51). Mechanistically, previous studies have reported a crucial role of CD4^{+} T cells for the optimal induction of cytotoxic CD8 T-cell responses or the activation of IFNγ-releasing macrophages (52–54). Flow cytometric–based profiling of the tumor microenvironment (TME) revealed that the adoptive transfer of CICR215W-specific T cells led to an increased abundance of T cells in the tumor. This was likely due to an increased T-cell recruitment by Cxcl9-producing monocyte-derived myeloid cells and IFNγ-dependent MHCII upregulation in the TME. Combining the locoregional T-cell transfer with radiation or ICB, improved survival was observed (**Fig. 4**;

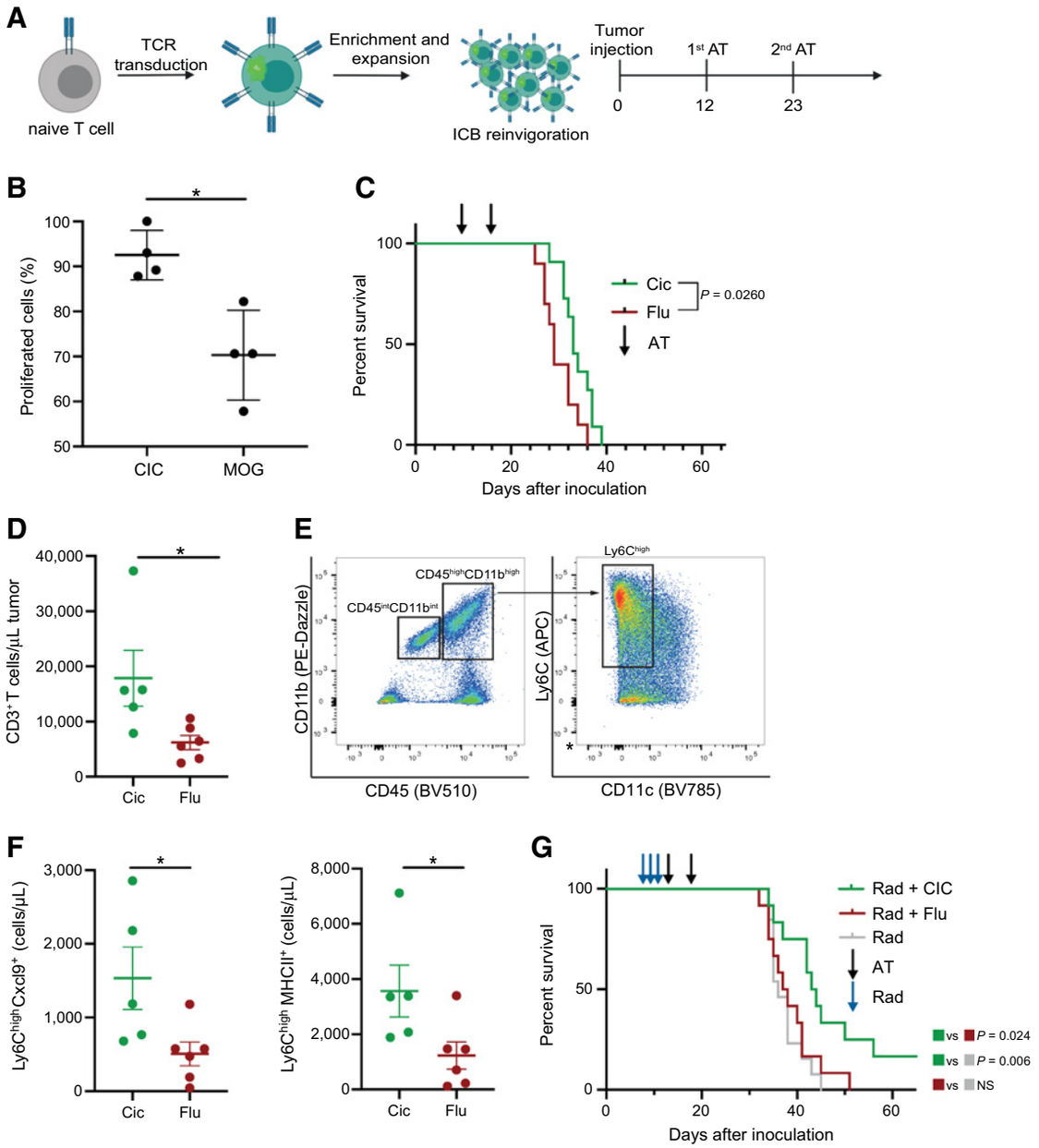

Figure 4.

Adoptive transfer of α-CICR215W-TCR T cells targeting CicR215W mutated A2.DR1 gliomas. **A,** Experimental overview: Activated A2.DR1 T cells were transduced with the α-CICR215W-TCR TCR coexpressing GFP and subsequently enriched and expanded for intraventricular injection in A2.DR1 glioma-bearing mice. **B,** *In vivo* T-cell proliferation of α-CICR215W-TCR T cells in A2.DR1 mice vaccinated with the CICR215W peptide or MOG measured by Cell Trace Far Red dilution. **C,** Kaplan–Meier curve of A2.DR1 glioma-bearing mice after 2 intraventricular adoptive transfers (AT) of α-CICR215W-TCR T cells and α-Flu-TCR T cells. $n = 10$ for Flu and $n = 11$ for CIC. **D,** Abundance of $CD45^+$, $CD3^+$ T cells in the tumor of CICR215W-reactive T cells or Flu-reactive T cell–treated mice. **E,** FACS gating for $Ly6C^{high}$ monocyte-derived myeloid cells. **F,** Abundance of Cxcl9 and MHCII expressing $Ly6C^{high}$ monocyte-derived macrophages. **D** and **E,** $n = 5$ for CIC and $n = 6$ for Flu. **G,** Kaplan–Meier curve of irradiated (total dose 12 Gy) A2.DR1 glioma-bearing mice after 2 intraventricular ATs of α-CICR215W-TCR T cells and α-Flu-TCR T cells. $n = 13$ for Rad, $n = 12$ for Flu (irrelevant control), and $n = 12$ for CIC. **B, D,** and **F,** Data are represented as mean ± SEM, statistical significance was determined by unpaired two-tailed Student *t* test. **C** and **G,** Statistical significance was determined by log-rank Mantel–Cox test. NS, not significant.

Supplementary Fig. S3F). The relevance of myeloid cell–derived T cell attracting chemokines for immunotherapy has been reported previously (55). Also, other reports have already shown profound preclinical responses targeting surface markers on intracranial tumor cells in immune-deficient mice (31, 32). However, a $CD4^+$ T cell–driven immune response is likely to be reliant on a fully competent immune system, as used in our model, to elicit sustained antitumor immunity ultimately via cytotoxic T cells. The microenvironmental fine-tuning capacity of $CD4^+$ T cells could potentially be further amplified by stimulating an increased inflammatory

TME using combinatorial (immuno)therapy approaches including immunoadjuvants, combination with cytotoxic TCR-transgenic T-cell therapy, or depletion of immunosuppressive stromal cells. On a broader level our data suggest that genetic alterations of driver genes—beyond tumor-intrinsic prognostic implications—result in the formation of clonal neoepitopes that can be therapeutically exploited in the context of low–mutational load entities such as oligodendroglioma.

Authors' Disclosures

J.K. Sonner reports grants from Helmholtz International Graduate School for Cancer Research during the conduct of the study, as well as grants from Tandemförderung UKE outside the submitted work. F. Sahm reports other support from Illumina during the conduct of the study, as well as other support from Bayer outside the submitted work. L. Bunse reports grants from Dr. Rolf M. Schwiete Foundation, Swiss Cancer Foundation, Else Kröner Fresenius Foundation, German Research Foundation (SFB1389-TPB03), University Heidelberg Foundation, and Sibylle Assmus Foundation during the conduct of the study. No disclosures were reported by the other authors.

Authors' Contributions

M. Kilian: Conceptualization, resources, data curation, investigation, visualization, methodology, writing–original draft, writing–review and editing. **M. Friedrich:** Investigation, methodology. **K. Sanghvi:** Investigation, methodology. **E. Green:** Resources, methodology. **S. Pusch:** Resources, methodology. **D. Kawauchi:** Resources, methodology. **M. Löwer:** Data curation, software, formal analysis, writing–review and editing. **J.K. Sonner:** Methodology. **C. Krämer:** Investigation. **J. Zaman:** Investigation, methodology. **S. Jung:** Investigation, methodology. **M.O. Breckwoldt:** Methodology. **G. Willimksy:** Investigation, methodology. **S.B. Eichmüller:** Resources. **A. von Deimling:** Resources, writing–review and editing. **W. Wick:** Conceptualization, writing–review and editing. **F. Sahm:** Resources, formal analysis, writing–review and editing. **M. Platten:** Conceptualization, funding acquisition, writing–original draft, writing–review and editing. **L. Bunse:** Conceptualization, supervision, funding acquisition, writing–original draft, writing–review and editing.

Acknowledgments

We thank K. Jähne, A. von Landenberg, and M. Fischer for expert technical assistance. We thank A. Marturano for providing immunofluorescence images. We acknowledge the support by the Center for Preclinical Research, the Light Microscopy Facility, the Core Facility for Small Animal Imaging, the Genomics and Proteomics Core Facility and Flow Cytometry Core Facility at the German Cancer Research Center, and the Flow Cytometry Core Facility at the Medical Faculty Mannheim of the Heidelberg University. We acknowledge the support in biostatistics by T. Holland-Letz. This work was supported by grants from the Dr. Rolf M. Schwiete Foundation, the German Ministry of Education and Science (National Center for Tumor Diseases Heidelberg NCT 3.0 program 'Precision immunotherapy of brain tumors' and the DKTK program), the Deutsche Forschungsgemeinschaft (DFG, German Research Foundation) – Project-ID 404521405, SFB 1389 - UNITE Glioblastoma, Work Package B01, to M. Platten; the Swiss Cancer Foundation, the Else Kröner Fresenius Foundation, the University Heidelberg Foundation, and the Sibylle Assmus Foundation to L.Bunse; the Deutsche Forschungsgemeinschaft (DFG, German Research Foundation) – Project-ID 404521405, SFB 1389 - UNITE Glioblastoma, Work Package B03) to L. Bunse and S. Pusch; the Helmholtz International Graduate School for Cancer Research to M. Kilian, K. Sanghvi, and J.K. Sonner; the *Landesgraduiertenförderung* (LGF) to M. Kilian; the Heidelberg Medical Faculty to L. Bunse; and the Mildred-Scheel doctoral program of the German Cancer Aid to C. Krämer and M.O. Breckwoldt was supported by the Else Kröner Fresenius Foundation and the Deutsche Forschungsgemeinschaft (DFG, German Research Foundation) – Project-ID 404521405, SFB 1389 - UNITE Glioblastoma, Work Package C03.

The costs of publication of this article were defrayed in part by the payment of page charges. This article must therefore be hereby marked *advertisement* in accordance with 18 U.S.C. Section 1734 solely to indicate this fact.

Received May 23, 2021; revised September 15, 2021; accepted October 28, 2021; published first November 15, 2021.

References

1. Yu JX, Upadhaya S, Tatake R, Barkalow F, Hubbard-Lucey VM. Cancer cell therapies: the clinical trial landscape. Nat Rev Drug Discov 2020;19:583–4.
2. Engelhardt B, Vajkoczy P, Weller RO. The movers and shapers in immune privilege of the CNS. Nat Immunol 2017;18:123–31.
3. Sampson JH, Gunn MD, Fecci PE, Ashley DM. Brain immunology and immunotherapy in brain tumours. Nat Rev Cancer 2020;20:12–25.
4. Vogelstein B, Papadopoulos N, Velculescu VE, Zhou S, Diaz LA, Kinzler KW. Cancer genome landscapes. Science 2013;339:1546–58.
5. Louis DN, Perry A, Reifenberger G, von Deimling A, Figarella-Branger D, Cavenee WK, et al. The 2016 WHO classification of tumors of the central nervous system: a summary. Acta Neuropathol 2016;131:803–20.
6. Schumacher T, Bunse L, Pusch S, Sahm F, Wiestler B, Quandt J, et al. A vaccine targeting mutant IDH1 induces antitumour immunity. Nature 2014; 512:324–7.
7. Pellegatta S, Valletta L, Corbetta C, Patanè M, Zucca I, Riccardi Sirtori F, et al. Effective immuno-targeting of the IDH1 mutation R132H in a murine model of intracranial glioma. Acta Neuropathol Commun 2015;3:4.
8. Platten M, Schilling D, Bunse L, Wick A, Bunse T, Riehl D, et al. A mutation-specific peptide vaccine targeting IDH1R132H in patients with newly diagnosed malignant astrocytomas: a first-in-man multicenter phase I clinical trial of the German Neurooncology Working Group (NOA-16). J Clin Oncol 2018;36:2001.
9. Ochs K, Ott M, Bunse T, Sahm F, Bunse L, Deumelandt K, et al. K27M-mutant histone-3 as a novel target for glioma immunotherapy. Oncoimmunology 2017; 6:e1328340.
10. Mueller S, Taitt JM, Villanueva-Meyer JE, Bonner ER, Nejo T, Lulla RR, et al. Mass cytometry detects H3.3K27M-specific vaccine responses in diffuse midline glioma. J Clin Invest 2020;130:6325–37.
11. Chheda ZS, Kohanbash G, Okada K, Jahan N, Sidney J, Pecoraro M, et al. Novel and shared neoantigen derived from histone 3 variant H3.3K27M mutation for glioma T cell therapy. J Exp Med 2018;215:141–57.
12. Keskin DB, Anandappa AJ, Sun J, Tirosh I, Mathewson ND, Li S, et al. Neoantigen vaccine generates intratumoral T cell responses in phase Ib glioblastoma trial. Nature 2019;565:234–9.
13. Hilf N, Kuttruff-Coqui S, Frenzel K, Bukur V, Stevanović S, Gouttefangeas C, et al. Actively personalized vaccination trial for newly diagnosed glioblastoma. Nature 2019;565:240–5.
14. Yip S, Butterfield YS, Morozova O, Chittaranjan S, Blough MD, An J, et al. Concurrent CIC mutations, IDH mutations, and 1p/19q loss distinguish oligodendrogliomas from other cancers. J Pathol 2012;226:7–16.
15. Bettegowda C, Agrawal N, Jiao Y, Sausen M, Wood LD, Hruban RH, et al. Mutations in CIC and FUBP1 contribute to human oligodendroglioma. Science 2011;333:1453–5.
16. Sahm F, Koelsche C, Meyer J, Pusch S, Lindenberg K, Mueller W, et al. CIC and FUBP1 mutations in oligodendrogliomas, oligoastrocytomas and astrocytomas. Acta Neuropathol 2012;123:853–60.
17. Bunda S, Heir P, Metcalf J, Li ASC, Agnihotri S, Pusch S, et al. CIC protein instability contributes to tumorigenesis in glioblastoma. Nat Commun 2019; 10:661.
18. Yang R, Chen LH, Hansen LJ, Carpenter AB, Moure CJ, Liu H, et al. Cic loss promotes gliomagenesis via aberrant neural stem cell proliferation and differentiation. Cancer Res 2017;77:6097–108.
19. Pajot A, Michel M-L, Fazilleau N, Pancré V, Auriault C, Ojcius D M, et al. A mouse model of human adaptive immune functions: HLA-A2.1-/HLA-DR1-transgenic H-2 class I-/class II-knockout mice. Eur J Immunol 2004;34:3060–9.
20. Shultz LD, Lyons BL, Burzenski LM, Gott B, Chen X, Chaleff S, et al. Human lymphoid and myeloid cell development in NOD/LtSz- scid IL2R γ null mice engrafted with mobilized human hemopoietic stem cells. J Immunol 2005;174: 6477–89.
21. Andreatta M, Nielsen M. Gapped sequence alignment using artificial neural networks: application to the MHC class I system. Bioinformatics 2016;32:511–7.

22. Nielsen M, Lundegaard C, Worning P, Lauemøller SL, Lamberth K, Buus S, et al. Reliable prediction of T-cell epitopes using neural networks with novel sequence representations. Protein Sci 2003;12:1007–17.
23. Reynisson B, Barra C, Kaabinejadian S, Hildebrand WH, Peters B, Nielsen M. Improved prediction of MHC II antigen presentation through integration and motif deconvolution of mass spectrometry MHC eluted ligand data. J Proteome Res 2020;19:2304–15.
24. Zuckermann M, Hovestadt V, Knobbe-Thomsen CB, Zapatka M, Northcott PA, Schramm K, et al. Somatic CRISPR/Cas9-mediated tumour suppressor disruption enables versatile brain tumour modelling. Nat Commun 2015;6:1–9.
25. Schrörs B, Boegel S, Albrecht C, Bukur T, Bukur V, Holtsträter C, et al. Multi-omics characterization of the 4T1 murine mammary gland tumor model. Front Oncol 2020;10:1195.
26. Gu Z, Gu L, Eils R, Schlesner M, Brors B. Circlize implements and enhances circular visualization in R. Bioinformatics 2014;30:2811–2.
27. Suzuki H, Aoki K, Chiba K, Sato Y, Shiozawa Y, Shiraishi Y, et al. Mutational landscape and clonal architecture in grade II and III gliomas. Nat Genet 2015;47:458–68.
28. Louis DN, Ellison DW, Brat DJ, Aldape K, Capper D, Hawkins C, et al. cIMPACT-NOW: a practical summary of diagnostic points from Round 1 updates. Brain Pathol 2019;29:469–72.
29. Draaisma K, Wijnenga MMJ, Weenink B, Gao Y, Smid M, Robe P, et al. PI3 kinase mutations and mutational load as poor prognostic markers in diffuse glioma patients. Acta Neuropathol Commun 2015;3:88.
30. Vora P, Venugopal C, Salim SK, Tatari N, Bakhshinyan D, Singh M, et al. The rational development of CD133-targeting immunotherapies for glioblastoma. Cell Stem Cell 2020;26:832–44.
31. Theruvath J, Sotillo E, Mount CW, Graef CM, Delaidelli A, Heitzeneder S, et al. Locoregionally administered B7-H3-targeted CAR T cells for treatment of atypical teratoid/rhabdoid tumors. Nat Med 2020;26:712–9.
32. Donovan LK, Delaidelli A, Joseph SK, Bielamowicz K, Fousek K, Holgado BL, et al. Locoregional delivery of CAR T cells to the cerebrospinal fluid for treatment of metastatic medulloblastoma and ependymoma. Nat Med 2020;26:720–31.
33. Braumüller H, Wieder T, Brenner E, Aßmann S, Hahn M, Alkhaled M, et al. T-helper-1-cell cytokines drive cancer into senescence. Nature 2013;494:361–5.
34. Kreiter S, Vormehr M, van de Roemer N, Diken M, Löwer M, Diekmann J, et al. Mutant MHC class II epitopes drive therapeutic immune responses to cancer. Nature 2015;520:692–6.
35. Brown CE, Aguilar B, Starr R, Yang X, Chang W-C, Weng L, et al. Optimization of IL13Rα2-targeted chimeric antigen receptor T cells for improved anti-tumor efficacy against glioblastoma. Mol Ther 2018;26:31–44.
36. Aslan K, Turco V, Blobner J, Sonner JK, Liuzzi AR, Núñez NG, et al. Heterogeneity of response to immune checkpoint blockade in hypermutated experimental gliomas. Nat Commun 2020;11:931.
37. Reardon DA, Gokhale PC, Klein SR, Ligon KL, Rodig SJ, Ramkissoon SH, et al. Glioblastoma eradication following immune checkpoint blockade in an orthotopic, immunocompetent model. Cancer Immunol Res 2016;4:124–35.
38. Nam J, Son S, Park KS, Zou W, Shea LD, Moon JJ. Cancer nanomedicine for combination cancer immunotherapy. Nat Rev Mater 2019;4:398–414.
39. Guedan S, Ruella M, June CH. Emerging cellular therapies for cancer. Annu Rev Immunol 2019;37:145–71.
40. Brown CE, Alizadeh D, Starr R, Weng L, Wagner JR, Naranjo A, et al. Regression of glioblastoma after chimeric antigen receptor T-cell therapy. N Engl J Med 2016;375:2561–9.
41. Rafiq S, Hackett CS, Brentjens RJ. Engineering strategies to overcome the current roadblocks in CAR T cell therapy. Nat Rev Clin Oncol 2020;17:147–67.
42. Neelapu SS, Tummala S, Kebriaei P, Wierda W, Gutierrez C, Locke FL, et al. Chimeric antigen receptor T-cell therapy-assessment and management of toxicities. Nat Rev Clin Oncol 2018;15:47–62.
43. Li D, Li X, Zhou W-L, Huang Y, Liang X, Jiang L, et al. Genetically engineered T cells for cancer immunotherapy. Signal Transduct Target Ther 2019;4:35.
44. Fesnak AD, June CH, Levine BL. Engineered T cells: the promise and challenges of cancer immunotherapy. Nat Rev Cancer 2016;16:566–81.
45. Rapoport AP, Stadtmauer EA, Binder-Scholl GK, Goloubeva O, Vogl DT, Lacey SF, et al. NY-ESO-1-specific TCR-engineered T cells mediate sustained antigen-specific antitumor effects in myeloma. Nat Med 2015;21:914–21.
46. Robbins PF, Morgan RA, Feldman SA, Yang JC, Sherry RM, Dudley ME, et al. Tumor regression in patients with metastatic synovial cell sarcoma and melanoma using genetically engineered lymphocytes reactive with NY-ESO-1. J Clin Oncol 2011;29:917–24.
47. Bunse L, Pusch S, Bunse T, Sahm F, Sanghvi K, Friedrich M, et al. Suppression of antitumor T cell immunity by the oncometabolite (R)-2-hydroxyglutarate. Nat Med 2018;24:1192–203.
48. Patrizii M, Bartucci M, Pine SR, Sabaawy HE. Utility of glioblastoma patient-derived orthotopic xenografts in drug discovery and personalized therapy. Front Oncol 2018;8:23.
49. Alspach E, Lussier DM, Miceli AP, Kizhvatov I, DuPage M, Luoma AM, et al. MHC-II neoantigens shape tumour immunity and response to immunotherapy. Nature 2019;574:696–701.
50. Mumberg D, Monach PA, Wanderling S, Philip M, Toledano AY, Schreiber RD, et al. CD4+ T cells eliminate MHC class II-negative cancer cells in vivo by indirect effects of IFN-γ. Proc Natl Acad Sci U S A 1999;96:8633–8.
51. Tveita A, Fauskanger M, Bogen B, Haabeth OAW. Tumor-specific CD4+ T cells eradicate myeloma cells genetically deficient in MHC class II display. Oncotarget 2016;7:67175–82.
52. Ossendorp F, Mengedé E, Camps M, Filius R, Melief CJM. Specific T helper cell requirement for optimal induction of cytotoxic T lymphocytes against major histocompatibility complex class II negative tumors. J Exp Med 1998;187:693–702.
53. Corthay A, Skovseth DK, Lundin KU, Røsjø E, Omholt H, Hofgaard PO, et al. Primary antitumor immune response mediated by CD4+ T cells. Immunity 2005;22:371–83.
54. Haabeth OAW, Lorvik KB, Hammarström C, Donaldson IM, Haraldsen G, Bogen B, et al. Inflammation driven by tumour-specific Th1 cells protects against B-cell cancer. Nat Commun 2011;2:240.
55. House IG, Savas P, Lai J, Chen AXY, Oliver AJ, Teo ZL, et al. Macrophage-derived CXCL9 and CXCL10 are required for antitumor immune responses following immune checkpoint blockade. Clin Cancer Res 2020;26:487–504.